Turbulence, Heat and Mass Transfer 7

Redistribution of solid inclusions in the turbulent flow of metallurgical induction furnaces

M. Ščepanskis[1], A. Jakovičs[1] , B. Nacke[2] and E. Baake[2]

[1]*Laboratory for Mathematical Modelling of Environmental and Technological Processes, University of Latvia,*
Zeļļu iela 8, LV-1002 Rīga, Latvia, {mihails.scepanskis, andris.jakovics}@lu.lv

[2]*Institute of Electrotechnology, Leibniz University of Hanover,*
Wilhelm-Busch-Str. 4, D-30167 Hannover, Germany, {nacke, baake}@etp.uni-hannover.de

Abstract – The paper refers to the dynamics of solid inclusion in the turbulent flow of liquid metal in induction furnaces. The numerical analysis is carried out adopting LES-based Euler-Lagrange approach in the limit of dilute conditions. The model is verified with the original experimental technique, which deals with ferromagnetic particles in the flow of Wood's metal in the small induction crucible furnace (ICF) of the laboratory scale. This experiment confirms the satisfactory agreement with the proper numerical results. The admixing of carbon particles in ICF from the open surface of a melt is also simulated. The behaviour of the particles in the bulk of the flow is illustrated and compared with the industrial observation of the alloy's open surface.

1. Introduction

The present work addresses the solid particles' transportation in the recirculated flow of metal melt in industrial induction metallurgical furnaces (IMF). All of them (induction crucible furnace – ICF, channel induction furnace – CIF, and others) have the same physical principle of operation (*Dötsch, 2009*) and, consequently, the similar flow distribution in the active region. The alternating current in the inductor creates a magnetic field and induces alternating current in the conductive liquid metal. The interaction of induced current and magnetic field results in the Lorentz force, which drives the liquid away from the wall and forms the two-eddy structure. However, the power of IMFs is sufficiently high to produce a turbulent flow with a high Reynolds number (e.g. for laboratory ICF it is about 1e+5). Therefore the mentioned two vortices appear only in the time averaged case, but in practice at each moment the turbulent flow consists of numerous eddies with different sizes, however, the common structure of the flow remains quasistationary (statistically stationary). The cross section of the ICF and the mean eddies are schematically shown on Figure 1 a.

The results produced by k-ε turbulence model, with a standard set of constants, show the highest values of turbulent kinetic energy in the eddy centers and the lowest between the eddies. Such distribution is characteristic for the k-ε model even in the case of 3D transient simulation (*Umbrashko et al., 2006*). However, the experimental results by *Umbrashko et al. (2006)* and *Kirpo et al. (2007)* show that the maximum of the turbulent energy is between the vortices of the averaged flow and close to the wall of the crucible. The average flow velocity in this area is close to zero, therefore the turbulent pulsations of velocity are large there. *Umbrashko et al. (2006)* and *Kirpo et al. (2007)* showed that the Large Eddy Simulation (LES) should be used for flow modeling in such equipment to achieve more realistic results. As far as the mass and heat transfer in the zone between eddies depends on the resolution of the velocity pulsations, the LES has to be used also for the objectives set out in the current paper. The spectrum of the pulsations of the axial velocity between these eddies has a clear

low frequency maximum (*Umbrashko et al., 2006*). *Ščepanskis et al. (2011-a)* found the same maximum in the spectrum of the oscillations of the particle number in the zone between the mean eddies. However, the extreme parts of this spectrum differ from the spectrum of the flow velocity due to the inertial effects.

The flow inside the induction furnaces is sufficiently complex due to the presence of the electromagnetic (EM) forces. Therefore, the case described in this paper significantly differs from the well-studied turbulence in a pipe, a channel and other classical flows. It also differs from the turbulent flow in the gap between two counterrotating disks (the von Kármán flow) due to intensive axial pulsations between the main eddies near the wall that has already been discussed. Therefore, the behaviour of the particles in this type of a flow is interesting from an engineering point of view and yet has not been sufficiently researched. Moreover, the EM field directly influences the non-conducting particles in the conducting liquid within the penetration depth and transport them to the wall, which is another specific aspect of the considered system. The layer of significant EM field is sufficiently thin (about 20% of the radius of the crucible – $\delta/R = 0.2$). Due to the non-slip boundary conditions the flow velocity is zero at the wall and increases in a radial direction until it rapidly achieves the maximal value at the relative distance $\Delta/R = 0.04$ from the wall. $\delta > \Delta$, therefore the maximum of velocity is inside the layer of EM penetration. Obviously, particles preferentially move in the streamline of maximal velocity. Therefore the major part of the particles come frequently to the layer of significant EM field. The particle motion in turbulent flows without EM is well researched, but it is not possible to separate the large interior zone without EM field from the thin layer near the wall and one should consider the motion of the particles in the whole volume.

EM heating and melting is one of the most effective methods for melting and processing of conducting materials. However, there is a problem of the homogenization of alloying particles, which are mixed in a steel melt to improve properties like strength, hardness and wear resistance. It is important to achieve homogeneous admixtures' distribution to ensure a high quality of the alloy. Furthermore, it is desirable to reduce the time of mixing to decrease the energy consumptions and prevent the melt from overheating. Most impurities and alloying elements have higher melting temperatures than metal. Thereby the melt can contain admixtures as solid particles. *Ščepanskis et al. (2010)* investigated the particle homogenization in ICF numerically.

Obviously, it is desirable to investigate the particle distribution in such systems experimentally, at least to verify the numerical model. But metals often have very high melting temperatures. Moreover, the electric well-conductive materials are not optically transparent, but transparent liquids have low conductivity. *Sadoway & Szekely (1980)* tried to use transparent LiCl-KCl eutectic to reproduce the recirculation motion in an ICF, but they met with failure. EM field does not only produce the induced flow motion, but also heat up the liquid within the penetration depth. Thereby the thermal convection dominates in the low-conductive transparent liquids. In spite of the optimistic conclusions of *Sadoway & Szekely (1980)*, the non-published simulation, which is done by the authors of the present paper, shows that it is not possible to avoid the thermal motion by changing the EM conditions. Therefore this liquid cannot be used to produce such flow patterns. The only more or less successful method, developed by *Taniguchi & Brimacombe (1994*), provides an opportunity to investigate experimentally the rate of the particle deposition in a turbulent flow of liquid metal under EM force. However, because the results are obtained by cutting solidified liquid, it is impossible to receive any information about the dynamics of the process inside the melt using such experimental technique. Moreover, the presence of the

solidification front has an influence on the particles during the solidification and it is not clear, if this effect is negligible.

Finally, the present paper proposes the original experimental technique, which uses ferromagnetic particles. This experiment allowed to verify the numerical model. The technique and the results are described in details below.

Previously *McKee et al. (1999)* proposed the greatly simplified analytical model for the calculation of the non-conductive particle path in rotating magnetohydrodynamic flow within a long cylinder. Later *Kirpo et al. (2009)* used Fluent software to investigate the behaviour of the particle cloud in the turbulent flows inside the induction furnaces. This model was sufficiently rough: only drag, buoyancy and EM forces were taken into account for the calculations of the particle motion. The model used by Kirpo was enhanced through development of OpenFOAM software code: the Lagrange equation was supplemented with lift, acceleration and added mass forces. The significance of these forces was statistically proved by *Ščepanskis et al. (2011-b).*

2. Mathematical Model

The present model includes the simulation of the flow and the particle motion. The flow is driven by EM force and thermal buoyancy force in the Boussinesq approximation. The turbulence is calculated using the Large Eddy Simulation (LES) method with the isotropic Smagorinsky subgrid viscosity model. The solid inclusions are calculated adopting the LES-based Euler-Lagrange approach in the limit of dilute conditions (one-way coupling). This assumption is possible because the volume of the inclusions does not exceed 1% of the liquid volume. The rigid spheres are also assumed. The Lagrange equation describes the motion of the inertia non-conductive spherical particles (*Ščepanskis et al., 2011-b*):

$$\underbrace{\left(1+\frac{C_\mathrm{A}}{2}\frac{\rho_\mathrm{f}}{\rho_\mathrm{p}}\right)\frac{\mathrm{d}\boldsymbol{u}_\mathrm{p}}{\mathrm{d}t}}_{\mathrm{d}\overline{u}_\mathrm{p}/\mathrm{d}t+\text{added mass force}}=\underbrace{C_\mathrm{D}\cdot\boldsymbol{U}}_{\text{drag force}}+\underbrace{\left(1-\frac{\rho_\mathrm{f}}{\rho_\mathrm{p}}\right)\boldsymbol{g}}_{\text{buoyancy force}}-\underbrace{\frac{3}{8\rho_\mathrm{p}}\mathbf{Re}\left(\boldsymbol{j}_0\times\boldsymbol{B}_0^*\right)}_{\text{EM force}}+\underbrace{\frac{\rho_\mathrm{f}}{\rho_\mathrm{p}}C_\mathrm{L}\boldsymbol{\xi}}_{\text{lift force}}+\underbrace{\left(1+\frac{C_\mathrm{A}}{2}\frac{\rho_\mathrm{f}}{\rho_\mathrm{p}}\right)\frac{\mathrm{D}\boldsymbol{u}_\mathrm{f}}{\mathrm{D}t}}_{\text{acceleration + added mass}}, \quad (1)$$

where $\boldsymbol{U}=\boldsymbol{u}_\mathrm{f}-\boldsymbol{u}_\mathrm{p}$, $\boldsymbol{u}_\mathrm{f}$ and $\boldsymbol{u}_\mathrm{p}$ are liquid and particle velocities respectively, ρ_f and ρ_p are liquid and particle density respectively, $\boldsymbol{g}$ is free fall acceleration; $\boldsymbol{j}_0$ is the amplitude of current density, $\boldsymbol{B}_0^*$ is complex conjugated for the amplitude of magnetic flux, $\boldsymbol{\xi}=\boldsymbol{U}\times(\nabla\times\boldsymbol{U})$; $C_\mathrm{A}(\mathrm{d}U/\mathrm{d}t,U)$, $C_\mathrm{D}(U)$ and $C_\mathrm{L}(U)$ are acceleration, drag and lift force coefficients respectively. The relevant approximations for the forces are chosen on the basis of the statistical analysis of the non-dimensional parameters (particle Reynolds number, shear stress and acceleration parameter).

It should be also mentioned that only the filtered velocity in the LES framework is known, and the isotropy of the subgrid part is assumed. Despite the calculation of the individual trajectories of particles, the analysis will be carried out for the cloud, therefore the unfiltered isotropic part of velocity should not influence the common results significantly.

As far as the hydrodynamics is simulated using the open source OpenFOAM software, the coupled Lagrange block is also programmed by means of OpenFOAM libraries. The particle tracking library is supplemented with EM, lift, acceleration and added mass forces. Thereby the Lagrange equation becomes non-linear. To ensure the convergence the hydrodynamic time step was split into various Lagrange time steps (LTS). The non-linear factors in the Lagrange equation are approximated with the values that correspond to the previous LTS (the Pikar's method). The implicit scheme is used to solve the equation. Moreover, the OpenFOAM

algorithm does not take into account the collision of a particle with the wall in a situation when the size of the particle is larger than the size of a mesh element. If the distance between the particle centre and the wall is smaller than the radius, then the present model moves the particle to the distance of the radius from the wall at the end of the each LTS.

3. Experimental Verification

The small 9 cm wide and 10 cm high crucible (that is the height of the melt) and the 4 kHz generator were used for the experiment (Figure 1 a). The spiral inductor had 6 turns and was the same height as the crucible. The 432 A current was applied in the inductor that corresponds to the induced power of 1.3 kW. The crucible was filled with the Wood's metal (50% Bi – 26.7% Pb – 13.3% Sn – 10% Cd eutectic), which becomes liquid at 70°C.

10.5 g of the spherical iron particles with diameter 250-350 μm were placed on the open surface of the liquid metal that generally corresponds to the industrial case of the admixing of alloying particles in ICF. The power of the furnace was switched on when the particles were already on the surface, it was done in the attempt to reduce the operation time of the furnace and thereby avoid the Wood's metal from dangerous overheating. Obviously, this case differs from industrial conditions, where the inclusions are usually placed on the surface of the already stirring metal. However, the measurements of the particle concentration were carried out at 11 s, when the transition regime of about 6 s had already passed. The local 4 ml probes of the particle laden Wood's metal were taken. Table 1 contains the comparison of the conditions in the experiment and the simulation. The iron particles were collected from the liquid sample using a strong permanent magnet and counted after that.

Table 1: Comparison of the conditions in the experiment and the simulation.

	experiment	simulation
number (mass) of the particles	10.5±0.1 g (~1e+4 particles)	83 635 particles
size of the particles	250 – 350 μm	300 μm
material (density) of the particles	iron (Fe)	iron (7 874 kg/m^3)
volume of the sample (experiment)	4±1 ml	-
correspondence of the experimental and simulated results	number of particles in the sample	(number of particles in the proper region) × (vol. of the sample) / (volume of the proper region)

Generally, the time dependent EM force should be written as follows (the average expression of the force is placed in the equation (1)):

$$\boldsymbol{f} = -\frac{3}{2}\frac{\sigma'' - \sigma'}{2\sigma'' + \sigma'}(\boldsymbol{j} \times \boldsymbol{B}) + \frac{\mu - \mu_0}{4\mu\mu_0}\nabla B^2, \qquad (2)$$

where $\boldsymbol{j}(t) = \boldsymbol{j}_0 \sin(\omega t + \varphi)$ and $\boldsymbol{B}(t) = \boldsymbol{B}_0 \sin(\omega t + \varphi)$ are time dependent current density and magnetic flux respectively, σ'' and σ' are the conductivity of the liquid and the particle

respectively, μ and μ_0 are the magnetic permeability of the particle and a vacuum respectively. The poor conductive ($\sigma' \ll \sigma''$) inclusions are usually used in the metallurgical applications, and they are non-magnetic ($\mu = \mu_0$). Thereby the equation (2) is reduced to the following expression:

$$\boldsymbol{f}_1 = -\frac{3}{4}(\boldsymbol{j} \times \boldsymbol{B}) = -\frac{3}{4\mu_0}\left((\boldsymbol{B}\nabla)\boldsymbol{B} - \frac{1}{2}\nabla B^2\right). \quad (3)$$

In the area of the maximal magnetic flux – at the middle of the inductor – B_r and B_φ are negligible. Therefore the first term in (3) can be reduced to $3/(4\mu_0)\cdot \boldsymbol{e}_z \cdot B_z \cdot \partial B_z/\partial z$ that is also negligible, because $\partial B_z/\partial z \approx 0$. Thus, the term $(\boldsymbol{B}\nabla)\boldsymbol{B}$ is much less than the second term in (3) at the middle of the inductor:

$$\boldsymbol{f}_1 \approx \frac{3}{8\mu_0}\cdot\nabla B^2. \quad (4)$$

However, the iron particles are used in the experiment. Iron is a good conductor ($\sigma' > \sigma''$) and a ferromagnetic material ($\mu \gg \mu_0$), but due to the partial wetting and the transitional resistance we can assume the equal conductivity of the particle and the liquid. Therefore for this type of particles equation (2) can be reduced to

$$\boldsymbol{f}_2 = \frac{1}{2\mu_0}\cdot\nabla B^2. \quad (5)$$

Apparently, the equations (4) and (5) shows that $f_1 \approx f_2$ at the middle of inductor. The results of the EM simulation on Figure 1 b also confirm the coincidence of the forces in the middle zone of the crucible, however, $f_2 \approx 3/2\, f_1$ in the zone of the flow vortices. Despite the non-critical differences between the forces f_1 and f_2 in the upper and lower eddies, it is possible to conclude that the iron particles can be used as the rough physical model of the typical metallurgical inclusions in the induction furnaces.

Figure 1 c provides comparison of the experimental results and the appropriate simulation. The simulation was carried out for the non-conductive and non-magnetic particles that corresponds to f_1. However, it must be noted that the iron particles, which are well-conductive and ferromagnetic, have been used in the experiment. The conditions and the rest EM parameters in the simulation are the same as in the physical experiment. 3 curves on the Figure 1 c correspond to the radial distribution of the inclusions at different depths: 3 cm (upper eddy), 5 cm (middle of the crucible) and 7 cm (lower eddy) from the surface. Notwithstanding the different conductivity and magnetic permeability of the inclusions, the experimental and simulated curves are in the satisfactory agreement to each other in all points except one: on the axis of symmetry in the zone of the upper eddy. This fact confirms the hypothesis discussed above and it is possible to use the iron particles as the physical model of non-conductive metallurgical inclusions.

However, two things should be additionally discussed concerning the results on Figure 1 c. 1) Unfortunately, no explanation has been obtained regarding the significant difference between experimental and simulated results in one point – on the symmetry axis in the upper part of the crucible. The experimental technology was quite rough and only 3 series of experiments yield the results on the upper curve of Figure 1 c. At the same time other experimental curves on Figure 1 c are drawn taking into account 4 – 10 experimental series. Therefore the problematic experimental point is the less reliable one compared to others. 2) The clustering of the particles on the wall in the zone of upper eddy was observed in the experiment. The authors believe that these clusters, which by the way contain the great

number of particles, are formed due to EM force, which holds the particles on the wall. The simulation also shows the concentration of the inclusions on the wall. However, this clustering effect was obviously enforced by poor wetting and the surface tension on the liquid metal – particle – wall interface. To the extent that the clustered inclusions were held on the wall, these particles did not get into the samples and did not influence the experimental results. Therefore, the particles, which were situated directly on the wall, were removed from the simulated data on Figure 1 c.

Thus it is possible to conclude that 1) the numerical model is in the satisfactory agreement with the experimental results; 2) it is convenient to use the iron particles as a physical model of non-conductive particles in conductive liquid in vicinity of an EM field.

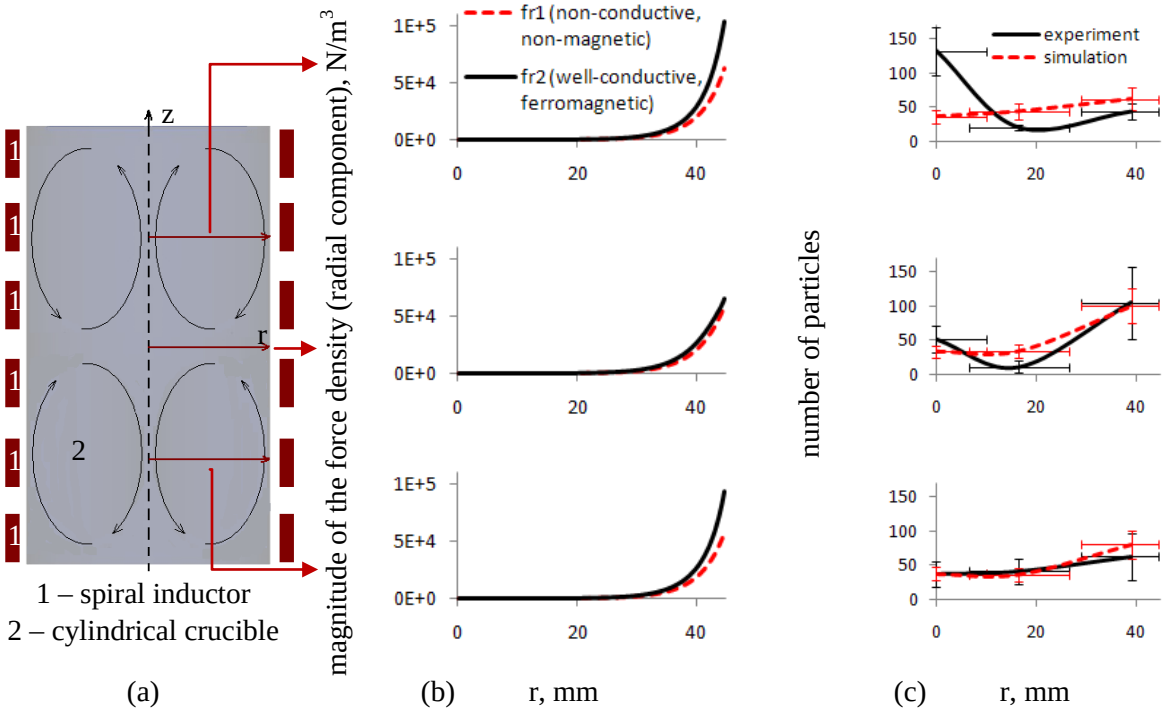

Figure 1: (a) scheme of ICF; (b) magnitude of the force density (radial component) in the case of non-conductive & non-magnetic and well-conductive & ferromagnetic particles (see equations (3) and (5) respectively); (c) the distribution of spherical 300±50 μm inclusions in ICF at 11±2 s from the beginning of stirring (quasi-stationary regime) at different depths from the surface (see the scheme of the crucible on the left).

4. Results of the Simulation

Following the previous discussion, the numerical model was verified experimentally in the small laboratory scale ICF. Therefore it is possible to analyze the industrial full scale process numerically.

Carbon particles are the typical alloying inclusions in steel. According to the widespread induction technology, the carbon particles are placed on the open surface of the liquid metal in the same ICF, where it has been melted previously. Then the intensive turbulent flow of alloy mixed the solid particles into the melt in spite of their low density. Apparently, it is important to achieve the homogeneous distribution of the inclusions to ensure high quality of the alloy. Furthermore, it is desirable to reduce the time of mixing to decrease the energy consumptions and prevent the melt from excessive overheating. The carbon has a low

conductivity, and moreover, transitional resistance appears on the surface. Therefore the EM force is applied in the Lagrange equation (1) as for a non-conductive particle.

Figure 2 compares the simulation of the carbon admixing process in steel with the industrial observations. Since the liquid steel is not transparent and is extremely hot, it is possible to compare only the behaviour of the particles on the open surface of the steel during the initial stage of the process (Figure 2 – first and second rows). The results qualitatively agree, therefore the motion in the bulk of the crucible can be analyzed, which is invisible (Figure 2 – last row). Initially the flow drives the cloud of inclusions to the corner between the surface and the wall, subsequently the intensive flow takes it inside and moves along the wall to the middle zone of the crucible. As it was shown by *Umbrashko et al. (2006)*, the most intensive axial turbulent pulsations were observed exactly in this region. These pulsations carry out the exchange of the particles between the two mean eddies and thereby homogenize the distribution of the inclusions with the lapse of time. The homogenization of the particles with different densities and sizes between the eddies was analysed in detail by *Ščepanskis et al. (2010)*.

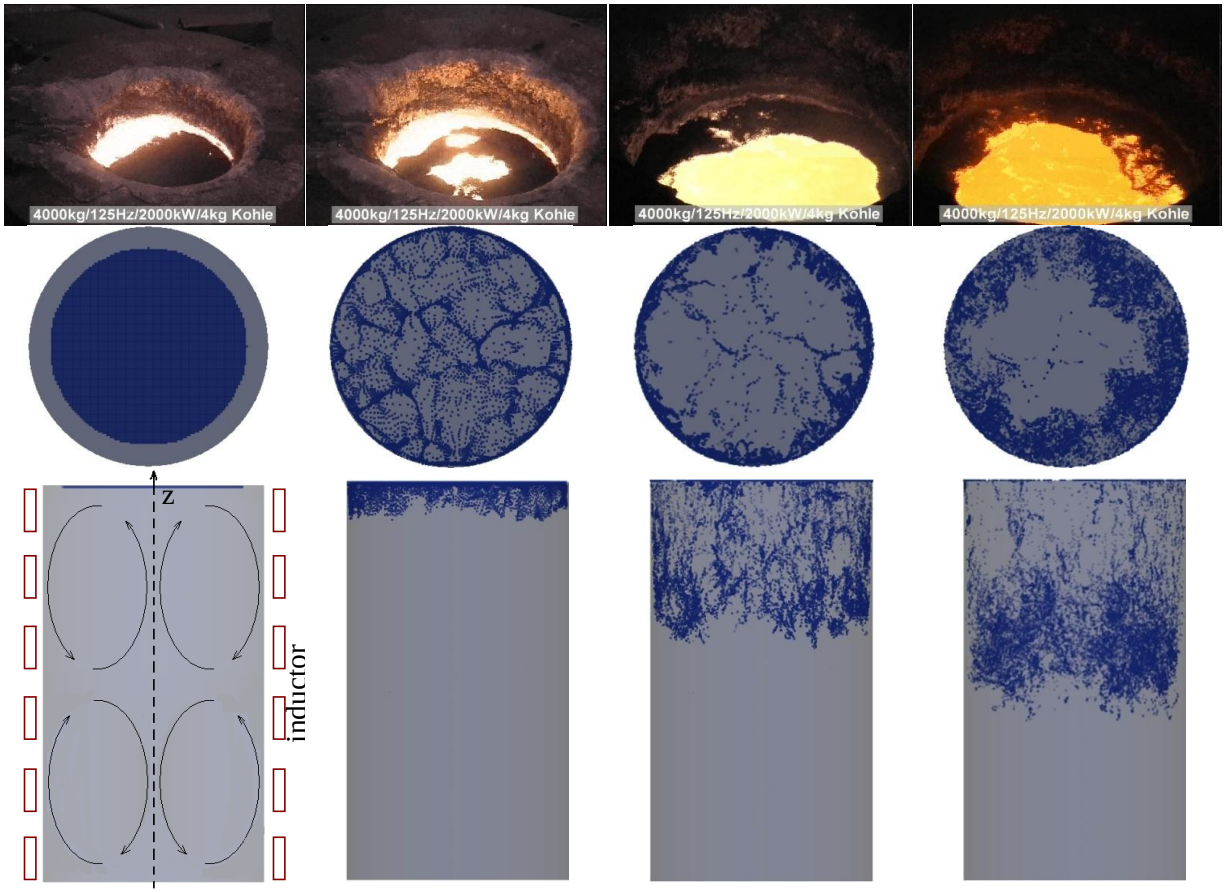

Figure 2: The admixing of the 100 μm carbon particles into the steel alloy in ICF. Snapshots of industrial process by Otto Junker GmbH (first row). Simulated results: view from the top of the furnace (second row); particles in the bulk of the flow, view from the side of furnace (last row).

5. Growth of the Inclusions

The redistribution of the equal-sized small solid inclusions is also analyzed in another type of induction furnace, namely CIF, last year (see e.g. the recent paper *Pavlovs et al., 2011*). However, the main problem concerning the CIF operation is the deposition of the impurities

like oxides as well as the erosion of the channel's walls. These processes can reduce the efficiency of the equipment significantly - up to breakdown (channel clogging). As it is shown in the Figure 3, the rate of the clogging dramatically increases, when the impurities start to deposit in the porous substance, like a sponge. This regime of the fast clogging, which reduces the active cross section of the channel very rapidly, attracts the attention of the operators of furnaces. The authors believe that this unfavourable sponge-like clogging can be fulfilled by depositing big particles, which previously grew in the bulk of the melt. Taking this hypothesis into account, it becomes clear that the simulation of the particles with invariable size is not completely relevant to the porous clogging problem and the size evolution of inclusions should be considered.

The process of the size evolution of inclusions can be provided by two different physical phenomena:

- diffusion limited Ostwald ripening (*Ratke & Voorhees, 2002*),
- collisions of the particles and clustering.

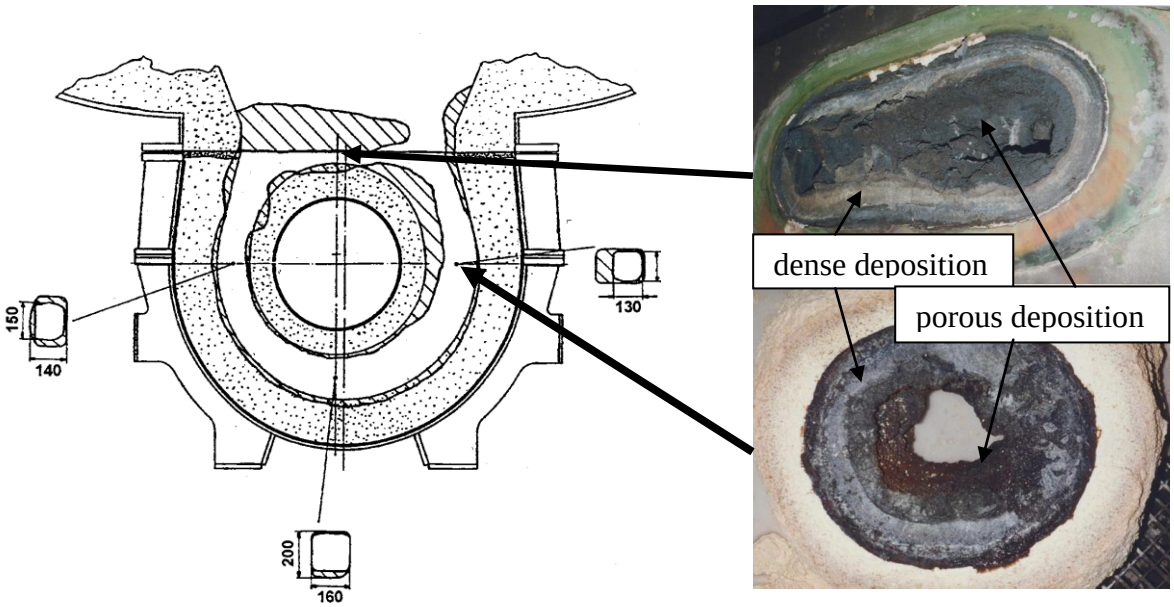

Figure 3: Left: the scheme of the build-up formations in the channel of 1200 kW cast-iron-inductor CIF after a 14 month long operation (*Drewek, 1996*). Right: the photos of clogged cross-sections of the neck and the channel of the CIF respectively (courtesy ABB Dortmund).

Ostwald ripening is the process of dissolution of small particles and the redeposition of the dissolved material on the surfaces of larger particles. This thermodynamically-driven spontaneous process occurs because larger particles are more energetically favoured than smaller particles. The system tries to lower its overall energy, so molecules on the surface of a small particle will diffuse into the solution. When all small particles do this, the free atoms in solution are supersaturated and condense on the surface of larger particles. Therefore, all smaller particles shrink, while larger particles grow, and overall the average size will increase. After an infinite amount of time, the entire population of particles will have become one, huge, spherical particle to minimize the total surface area. But due to EM force this asymptotical state will be not achieved and the particles with arbitrary size will be removed from the melt by deposition on the wall.

Table 2: Time to change twice the volume of a Al_2O_3 particle in a steel melt, assuming the relative supersaturation 0.472, which corresponds approximately to the transitions from working to weekend regime of the CIF operation. Results are calculated for 215 kW CIF, assuming the homogeny distributed inclusions with common volume concentration 1%, the concentration of the particles in each size group is assumed equal. The degree of turbulent energy dissipation rate is calculated equal to 1e-2 m^2/s^3. Table form *Ščepanskis et al. (2012)*

Diameter of particles, m	**Collision model** time, s	**Ostwald ripening (diffusion limited growth)** time, s
1e-7	1.42e+0	6.99e-1
1e-6	2.00e+1	6.66e+1
1e-5	2.03e+1	6.31e+3
1e-4	2.03e+1	6.28e+5

The collision model includes turbulent, Stokes and Brownian terms.

Recently, *Ščepanskis et al. (2012)* estimated the growth of the oxide inclusions in the CIF considering the diffusion limited growth and the collisions of the particles. The analyzed case simulated the transition from the working to the weekend regime of the CIF operation, when the temperature of the melt is usually changed from 100 K above the melting point of the steel (1883 K) to 40 K (1823 K). Table 2 shows the time, which is necessary to double the volume of the particle under the described conditions. If the weekend period is assumed about 2.2E+5 s, it becomes evident, that the described processes can increase the size of the inclusions significantly and, consequently, favour the porous clogging. Turbulent collisions will drive this process, if the concentration of the big particles is sufficient, but at the opposite case the particles will grow also within the model of diffusion limited process (Ostwald ripening). Moreover, due to the Ostwald ripening the smallest inclusions will rapidly achieve the size, when collision model gives significant results. Therefore the tracing of the inertia particles in CIF should be done, coupling it with the size evolution model. The authors plan to carry out this simulation in the future.

6. Conclusions

The iron particles can be used as a physical model for the tracking of non-conductive inclusions in ICF. The original experimental results are in a satisfactory agreement with the simulations. The described experimental technique is very useful, because the ferromagnetic particles can be easily separated from the liquid metal with the permanent magnet.

The numerical results of the carbon admixing from the open surface of the steel melt in ICF are in a good qualitative agreement with the industrial observation of the particle dynamics on the surface of the melt. Therefore the calculations can also give a relevant conception of the redistribution of the inclusion in the invisible bulk of the melt.

The estimations show that the average size of the inclusions can significantly increase during the weekend, when the furnace is switched to a lower power regime. This process can ensure the sponge-like clogging. The present estimations confirm the necessity of the particle tracking simulation in CIF, coupled with the size evolution model.

7. Acknowledgement

The contribution of M. Ščepanskis is sponsored by the European Social Fund within the project "Support for Doctoral Studies at University of Latvia".

References

1. E. Dötsch. *Inductive melting and holding*. Vulkan-Verlag, 2009.
2. A. Umbrashko, E. Baake, B. Nacke and A. Jakovics. Modeling of the turbulent flow in induction furnaces. *Metall. Mater. Trans. B*, 37B: 831-838, 2006.
3. M. Kirpo, A. Jakovičs, E. Baake and B. Nacke. Analysis of experimental and simulation data for the liquid metal flow in a cylindrical vessel. *Magnetohydrodynamics*, 43: 161-172.
4. M. Ščepanskis, A. Jakovičs, E. Baake and B. Nacke. The oscillations appearing during the process of particle homogenization in EM induced flow of ICF. In *8th International PAMIR Conference on Fundamental and Applied MHD*, 2: 653-657, 2011-a.
5. M. Ščepanskis, A. Jakovičs and B. Nacke. Homogenization of non-conductive particles in EM induced metal flow in a cylindrical vessel. *Magnetohydrodynamics*, 46: 413-423, 2010.
6. D. R. Sadoway and J. Szekely. A new experimental technique for the study of turbulent electromagnetically driven flows. *Metall. Trans. B*, 11B: 334-336, 1980.
7. S. Taniguchi and J. K. Brimacombe. Application of pinch force to the separation of inclusion particles from liquid steel. *ISIJ International*, 34: 722-731, 1994.
8. M. Ščepanskis, A. Jakovičs and E. Baake. Statistical analysis of the influence of forces on particles in EM driven recirculated turbulent flows. *J.Phys.:Conf.Ser.*, 333: 012015, 2011-b.
9. S. McKee, R. Watson, J. R. Cuminato and P. Moor. Particle-tracking within turbulent cylindrical electromagnetically-driven flow. *Int. J. Numer. Meth. Fluids*, 29: 59-74, 1999.
10. M. Kirpo, A. Jakovičs, E. Bake and B. Nacke. LES study of particle transport in turbulent recirculated liquid metal flows. *Magnetohydrodynamics*, 45: 439-450, 2009.
11. S. Pavlovs, A. Jakovičs, E. Baake, B. Nacke and M. Kirpo. LES modelling of turbulent flows, heat exchange and particle transport in industrial induction channel furnaces. Magnetohydrodynamics, 46: 399–412, 2011.
12. L. Ratke and P. W. Voorhees. *Growth and coarsening: Ostwald ripening in material processing*. Springer, 2002.
13. R. Drewek. *Verschleißmechanismen in Induktions-Rinnenöfen für Gußeisen und Aluminium.* Forschr.-Ber. VDI Reihe 21 Nr. 193, VDI-Verlag, 1996 (in German).
14. M. Ščepanskis, A. Jakovičs, M. Brics, E. Baake and B. Nacke. Simulation of growth and transportation of solid inclusions in induction furnaces. In *8th International Conference on Clean Steel*, on CD, 2012. In the book of abstracts: 26.